Research Article

Effect of synthesis conditions and composition on structural and phase states and electrical properties of nanogranular $(FeCoZr)_x(PZT)_{100-x}$ films $(30 \leq x \leq 85$ at.%)

Julia A. Fedotova[1]

1 *Institute for Nuclear Problems, Belarusian State University, 11 Bobruiskaya Str., Minsk 220006, Belarus*

Corresponding author: Julia A. Fedotova (Julia@hep.by)

Abstract

Granular films containing $Fe_{50}Co_{50}Zr_{10}$ alloy nanoparticles inside $Pb_{0,81}Sr_{0,04}(Na_{0,5}Bi_{0,5})_{0,15}(Zr_{0,575}Ti_{0,425})O_3$ (PZT) ferroelectric matrix possess a combination of functional magnetic and electrical properties which can be efficiently controlled by means of external electric or magnetic fields. The formation of the required granular structure in PZT matrix is only possible if synthesis is carried out in an oxygen-containing atmosphere leading to substantial oxidation of metallic nanoparticles. Thus an important task is to study the oxidation degree of metallic nanoparticles depending on synthesis conditions and the effect of forming phases on the electrical properties of the films.

The relationship between the structural and phase state and electrical properties of granular $FeCoZr)_x(PZT)_{100-x}$ films $(30 \leq x \leq 85$ at.%) synthesized in an oxygen-containing atmosphere at the oxygen pressure P_O in a range of $(2.4–5.0) \cdot 10^{-3}$ Pa has been studied using X-ray diffraction, EXAFS and four-probe electrical resistivity measurement.

Integrated comparative analysis of the structural and phase composition and local atomic order in $(FeCoZr)_x(PZT)_{100-x}$ films has for the first time shown the fundamental role of oxygen pressure P_O during synthesis on nanoparticle oxidation and phase composition. We show that the oxygen pressure being within $P_O = 3.2 \cdot 10^{-3}$ Pa an increase in x leads to a transition from nanoparticles of Fe(Co,Zr)O complex oxides to a superposition of complex oxides and α-FeCo(Zr,O) ferromagnetic nanoparticles (or their agglomerations). At higher oxygen pressures $P_O = 5.0 \cdot 10^{-3}$ Pa the nanoparticles undergo complete oxidation with the formation of the $(Fe_xCo_{1-x})_{1-\delta}O$ complex oxide having a Wurtzite structure.

The forming structural and phase composition allows one to explain the observed temperature dependences of the electrical resistivity of granular films. These dependences are distinguished by a negative temperature coefficient of electrical resistivity over the whole range of film compositions at a high oxygen pressure ($P_O = 5.0 \cdot 10^{-3}$ Pa) and a transition to a positive temperature coefficient of electrical resistivity at a lower oxygen pressure ($P_O = 3.2 \cdot 10^{-3}$ Pa) in the synthesis atmosphere and $x > 69$ at.% in the films. The transition from a negative to a positive temperature coefficient of electrical resistivity which suggests the presence of a metallic contribution to the conductivity is in full agreement with the X-ray diffraction and EXAFS data indicating the persistence of unoxidized α-FeCo(Zr,O) ferromagnetic nanoparticles or their agglomerations.

Keywords

granular nanocomposite films, ferroelectrics, X-ray diffraction analysis, electrical conductivity, EXAFS.

1. Introduction

Granular metal/dielectric films consisting of metal or alloy nanoparticles (Co, FeCo, FeNi etc.) inside a dielectric matrix (Al_2O_3, SiO_2) are distinguished by a unique combination of electrical, magnetoresistive, magnetic, optical and other properties [1–8]. For example they possess a high saturation magnetization (M_S up to 1800 A · m), low room-temperature coercive force (H_C < 4 kA/m), a large real part of magnetic permeability μ′ (up to 200 at frequencies of below 50 MHz) and variable electrical resistivity ρ over a wide range (10^{-2}–10 Ohm · m). Another advantages of granular nanocomposite films, taking into account their engineering applications including electronics, are acceptable mechanical properties and a high corrosion resistance.

Practically valuable granular materials include films containing $Fe_{50}Co_{50}$ alloy based nanoparticles inside a $Pb_{0,81}Sr_{0,04}(Na_{0,5}Bi_{0,5})_{0,15}(Zr_{0,575}Ti_{0,425})O_3$ **(PZT)** ferroelectric matrix. The ferroelectric nature of the PZT matrix seems to deliver the possibility of controlling the magnetic and electrical properties of FeCoZr/PZT films by applying either magnetic or electric fields.

Experimental studies [2] provide sound proof of the fact that the formation of metal/nonmetal films with a granular structure occurs by self-organization of the two phases provided these phases are mutually insoluble and the systems do not contain chemical compounds and have different surface energies. However the whole set of conditions required for the formation of a granular structure in the films is not the case for all metal/nonmetal (dielectric) combinations. In other words the use of complex oxides like PZT as matrices does not always allow synthesizing films with the required structure by deposition in an Ar inert gas atmosphere, even if the composition is below the percolation threshold x_C. Oxygen addition to the synthesis atmosphere is in this case the only experimentally proven possibility to stabilize the nanogranular structure of the films due to the formation of nanoparticles with a metallic core/oxide shell structure [9, 10].

Below we present experimental data on the relationship between the structural and phase state and electrical properties of $(FeCoZr)_x(PZT)_{100-x}$ films ($30 \leq x \leq 85$ at.%) grown in an oxygen containing atmosphere (P_O = (2.4–5.0) · 10^{-3} Pa). We studied $(FeCoZr)_x(PZT)_{100-x}$ films in three main composition ranges: below the percolation threshold ($x_{FeCoZr} < x_C$, 45 at.%), near x_C and beyond the percolation threshold ($x_{FeCoZr} > x_C$) [11].

2. Experimental

The 1–3 μm test films were deposited by ion beam sputtering at argon partial pressure in the chamber P_{Ar} = 1.1 · 10^{-1} Pa, a 170 mA plasma flux and a ~3500 V voltage. The working gas for target sputtering was 99.992 % pure argon. The oxygen partial pressure

was in the range P_O = 2.0–5.0 · 10^{-3} Pa. The substrates were made from sitall films and aluminum foil. Before the film deposition the targets were sputtered for 30 min. Then in order to improve adhesion of the deposited film to the substrate the substrate was ion beam cleaned for 20–30 min. The composite target was in the form of PZT wafers placed on a continuous wafer of $Fe_{45}Co_{45}Zr_{10}$ at.% metallic alloy. If this design of a target is used for sputtering the concentration ratio of the metallic and dielectric fractions deposited onto the substrate proves to be proportional to the ratio of the areas of the metallic alloy and the dielectric wafers on the opposite side of the target. Thus varying the number of dielectric wafers and the distance between them one can change the ratio of the volumes of the deposited metallic and dielectric layers between ~20 and ~80 at.% in one process cycle [1, 2].

X-ray diffraction analysis of the films deposited onto sitall substrates and aluminum foil was conducted on a Empyrean PANalytical diffractometer in CuK_α characteristic X-ray radiation with a graphite monochromator and an X'Celerator linear detector. The X-ray diffraction patterns were recorded at a 5 deg incidence angle relative to the specimen surface and by scanning in the reflection angle range 2Θ = 10–120 deg.

The local neighborhood of the cobalt, iron and zirconium ions in the films was studied by analyzing the X-ray near-edge structure (**XANES** spectroscopy) and the extended X-ray absorption fine structure (**EXAFS**). The XANES and EXAFS spectra were recorded with the use of an ID26 beam of the European Synchrotron Radiation Facility (ESRF) and a Petra III accelerator of Deutsches Elektronen Synchrotron (DESY). The absorption energy determination resolution was ~1.0 eV.

Electrical resistivity measurements were carried out with a four-probe potentiometric method at the linear section of the voltage-current curve using a High Field Measurement System (HFMS), Cryogenic Limited, for cryogenic electrical measurements in the 10–300 K range. The temperature in the cryostat near the test specimen was measured accurate to not worse than 0.001 K. The test specimens on sitall substrates were 2 mm wide and 10 mm in length, with indium Ohmic contacts ultrasonically soldered at the edges. The contact spacing was 7 ± 0.5 mm. The DC source and voltage meter was Keithley's Sub-Femtoamp Remote SourceMeter 6430 allowing high precision resistivity measurements in the range from 100 μOhm to 20 GOhm.

3. Results and discussion

3.1. X-ray structural analysis

Figure 1 shows X-ray diffraction patterns of the $(FeCoZr)_x(PZT)_{100-x}$ films ($35 \leq x \leq 81$ at.%) synthesized in an oxygen-containing atmosphere at two oxygen pressures (P_O = 2.4 · 10^{-3} and 3.7 · 10^{-3} Pa) on aluminum

foil substrates. The diffraction line seen in X-ray patterns *3–6* at 2Θ = 44.2–44.4 deg can be identified as the (110) plane reflection of the bcc lattice of α-FeCo(Zr,O) alloy [9, 12]. The intensity of this line is negligible for the $(FeCoZr)_{35}(PZT)_{65}$ film and increases gradually with an increase in x. This reflection line is heavily broadened, $\Delta(2\Theta)$ = 6.0 deg, due to the nanoscale size of the particles. All the X-ray patterns exhibit a broadened line at low reflection angles corresponding to a superimposition of the contributions from the PZT matrix [13] and iron oxides and/or cobalt ferrites [14, 15]. Comparison of X-ray patterns *1* and *6* in Fig. 1 c suggests that an increase in x leads to a shift of this line towards higher reflection angles 2Θ. This trend indicates an increase in the content of oxidized nanoparticles in the films (the presence of iron oxides and/or cobalt ferrites) and a decrease in the contribution from the PZT matrix. The de-
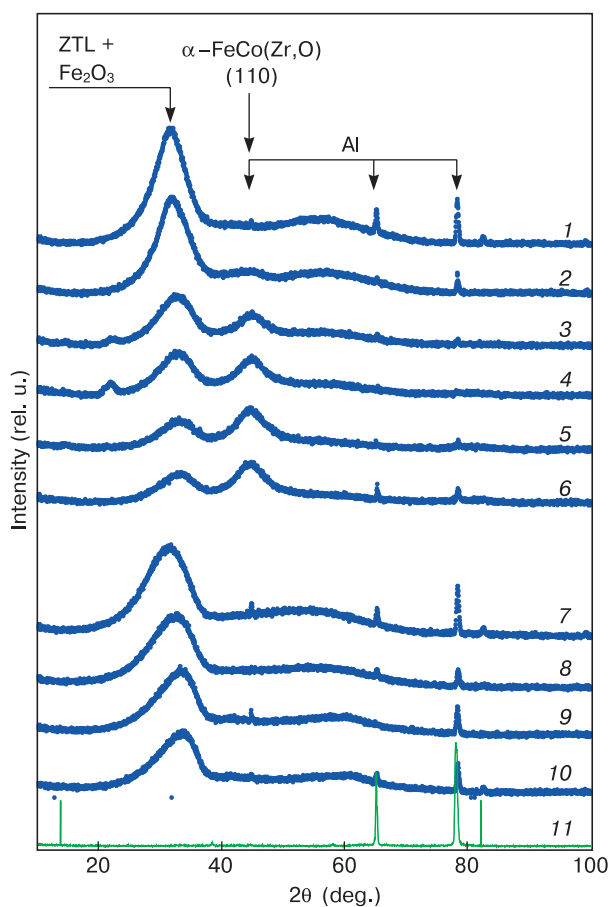
crease in the intensity of the lines for the PZT matrix and the increase in the intensity of the α-FeCo(Zr,O) lines with an increase in x are in full agreement with the change in the relation between the contents of the metallic and nonmetallic fractions in the films. The narrow reflections seen in the X-ray patterns at high reflection angles pertain to the aluminum substrate (Fig. 1, Curve *11*).

X-ray patterns *7–10* (Fig. 1) for the FeCoZr-PZT films synthesized at a higher oxygen pressure (P_O = 3.7 · 10^{-3} Pa) exhibits one dominating reflection at $2\Theta \approx$ 33 deg which is close to that of iron oxides [14]. However the (110) diffraction line of α-FeCo(Zr,O) is completely absent. This latter fact supports the assumption of the complete oxidation of FeCoZr metallic granules in the films during deposition in an oxygen-containing atmosphere at P_O = 3.7 · 10^{-3} Pa. Taking this conclusion into account one should note the good coincidence between the positions of the lines for completely oxidized FeCoZr nanoparticles in the X-ray diffraction patterns of the $(FeCoZr)_{81}(PZT)_{19}$, films deposited at two different oxygen pressures P_O = 2.4 · 10^{-3} and 3.7 · 10^{-3} Pa.

3.2. Local neighborhood of iron and cobalt ions in oxidized FeCoZr-PZT films

For a more complete understanding of the experimental results we present below a detailed analysis of the short-range order in the oxidized $(FeCoZr)_x(PZT)_{100-x}$ films as studied using Fe-, Co- and Zr-EXAFS spectroscopy. Fig. 2 shows typical EXAFS function modules after Fourier transformation for iron and cobalt taken from the most typical films with the compositions $(FeCoZr)_{50}(PZT)_{50}$ and $(FeCoZr)_{79}(PZT)_{21}$ (P_O = 2.4 · 10^{-3} Pa) synthesized in an Ar + O$_2$ atmosphere on aluminum foil substrates, for the $(FeCoZr)_{56}(PZT)_{44}$ and $(FeCoZr)_{84}(PZT)_{16}$ films (P_O = 3.2 · 10^{-3} Pa) and for the $(FeCoZr)_{56}(PZT)_{44}$ film (P_O = 5.0 · 10^{-3} Pa) deposited onto sitall substrates. For identification of the closest neighborhood of the iron and cobalt ions Fig. 2 also presents curves that are typical of the reference FeCoZr alloy film and the crystalline CoO, FeO and γ-Fe$_2$O$_3$ reference specimens.

As can be seen from Fig. 2 *a* for almost all the film compositions and P_O regardless of substrate type, iron ions are surrounded by oxygen ions. The only exclusion is the oxidized film with the highest experimental x, i.e., $(FeCoZr)_{84}(PZT)_{16}$, on a sitall substrate deposited at P_O = 3.2 · 10^{-3} Pa. There the iron ions and the cobalt ions are surrounded by metallic ions. On the contrary, most of the cobalt ions have metallic neighbors. As follows from the values of R for the cobalt absorption line peaks the oxygen ions are their closest neighbors only in films with compositions close to the percolation threshold x_C ($(FeCoZr)_{50}(PZT)_{50}$) deposited at P_O = 2.4 · 10^{-3} Pa.

One should specially mention the oxidized $(FeCoZr)_{56}(PZT)_{44}$ film deposited at P_O = 5.0 · 10^{-3} Pa. In this film the local neighborhood of iron and cobalt ions

Figure 1. Typical experimental X-ray patterns (dots) and Rietweld approximations (solid line) for $(FeCoZr)_x(PZT)_{100-x}$ films ($35 \leq x \leq 81$ at.% synthesized in an Ar + O$_2$ atmosphere on aluminum foil substrates: (*1*) $(FeCoZr)_{35}(PZT)_{65}$, P_O = 2.4 · 10^{-3} Pa; (*2*) $(FeCoZr)_{50}(PZT)_{50}$, P_O = 2.4 · 10^{-3} Pa; (*3*) $(FeCoZr)_{63}(PZT)_{37}$, P_O = 2.4 · 10^{-3} Pa; (*4*) $(FeCoZr)_{67}(PZT)_{33}$, P_O = 2.4 · 10^{-3} Pa; (*5*) $(FeCoZr)_{77}(PZT)_{23}$, P_O = 2.4 · 10^{-3} Pa; (*6*) $(FeCoZr)_{81}(PZT)_{19}$, P_O = 2.4 · 10^{-3} Pa; (*7*) $(FeCoZr)_{50}(PZT)_{50}$, P_O = 3.7 · 10^{-3} Pa; (*8*) $(FeCoZr)_{67}(PZT)_{33}$, P_O = 3.7 · 10^{-3} Pa; (*9*) $(FeCoZr)_{77}(PZT)_{23}$, P_O = 3.7 · 10^{-3} Pa; (*10*) $(FeCoZr)_{81}(PZT)_{19}$, P_O = 3.7 · 10^{-3} Pa; (*11*) aluminum foil.
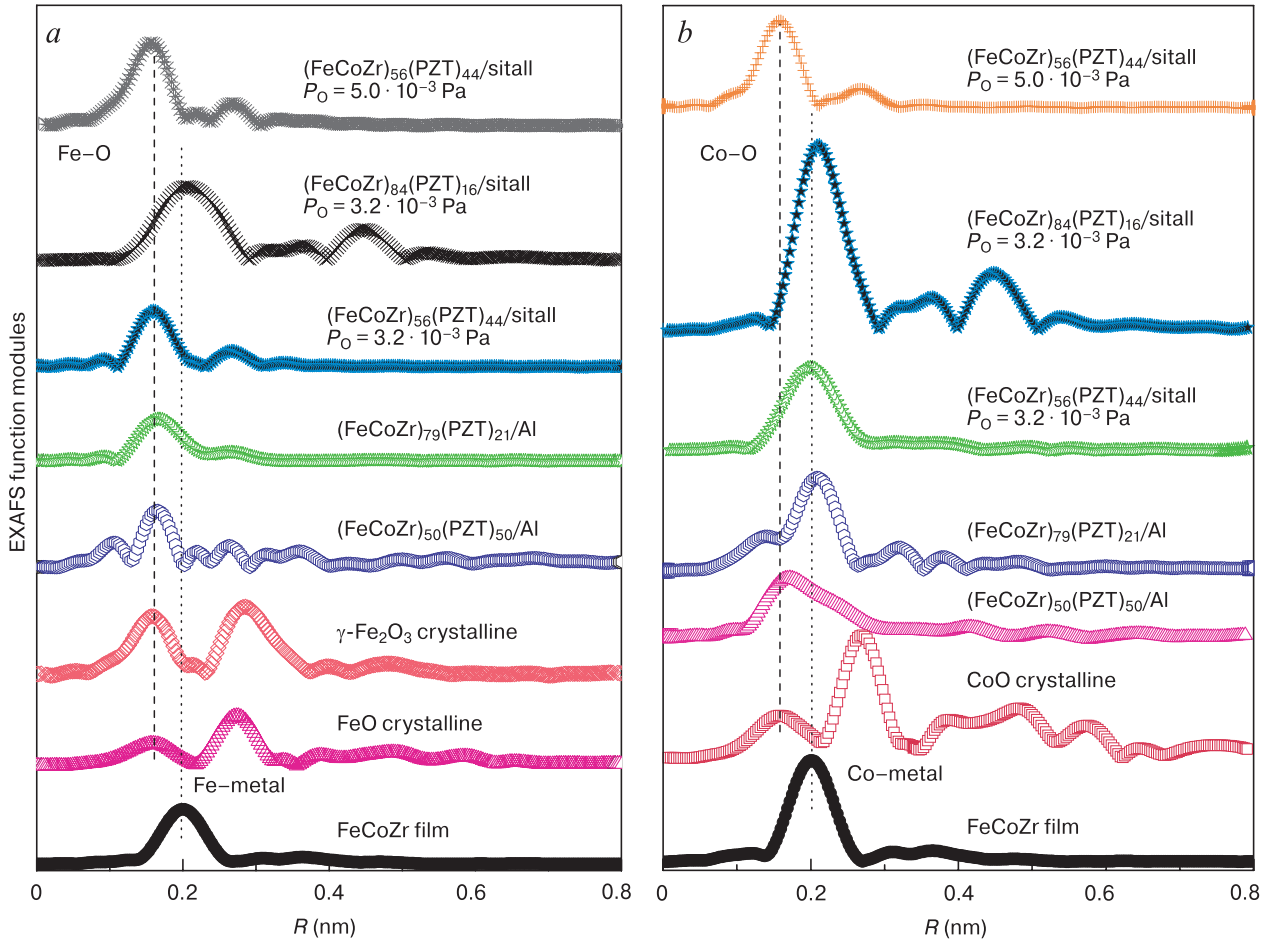
Figure 2. EXAFS function modules after Fourier transformation for absorption K edge of (*a*) iron and (*b*) cobalt for the FeCoZr alloy reference film and the oxidized films: $(FeCoZr)_{50}(PZT)_{50}$ and $(FeCoZr)_{79}(PZT)_{21}$ on an Al substrate ($P_O = 2.4 \cdot 10^{-3}$ Pa), $(FeCoZr)_{56}(PZT)_{44}$ and $(FeCoZr)_{84}(PZT)_{16}$ on a sitall substrate ($P_O = 3.2 \cdot 10^{-3}$ Pa), and $(FeCoZr)_{56}(PZT)_{44}$ on a sitall substrate ($P_O = 5.0 \cdot 10^{-3}$ Pa), and CoO, FeO and γ-Fe_2O_3 reference crystalline specimens.

consists of oxygen ions, i.e., the nanoparticles are completely oxidized.

The local oxygen ion neighborhood of iron and cobalt ions at $x \approx x_C$ ($(FeCoZr)_{50}(PZT)_{50}$) correlates well with the absence (or a but minor contribution) of the X-ray reflection line for the α-FeCo(Zr,O) alloy (Fig. 1, Curves *1* and *2*). This suggests an almost complete oxidation of the FeCoZr nanoparticles in the films having pre-percolation compositions. Beyond the percolation threshold the local neighborhood of the iron ions is typical of its oxides whereas the cobalt ions haven metallic neighbors (Fig. 2 *a* and *b* for the $(FeCoZr)_{79}(PZT)_{21}$ film. Taking into account the intense reflection line of the α-FeCo(Zr,O) alloy in the X-ray diffraction patterns of the $(FeCoZr)_{77}(PZT)_{23}$ and $(FeCoZr)_{81}(PZT)_{19}$ films (Fig. 1, Curves *5* and *6*), the difference in the local neighborhood of iron and cobalt can be attributed to the simultaneous presence of the α-FeCo(Zr,O) cobalt-rich metallic alloy and disordered iron oxides. This selective oxidation was discussed in detail earlier for oxidized FeCoZr–Al_2O_3 films [16, 17].

By and large the evolution of the structural and phase composition, more specifically, the oxidation of nanoparticles at different oxygen pressures P_O depending on the contribution from the metallic fraction x, can be accounted for as follows. According to Mossbauer data on granular nanocomposites [10, 17, 18], at the lowest oxygen pressure in the chamber during film deposition ($P_O = (2.4–3.2) \cdot 10^{-3}$ Pa) and $x < 67$ at.% the films usually contain superparamagnetic nanopartciles of the $Fe^{3+}(Co,Zr)O$ complex oxide (based on maghemite γ-Fe_2O_3 or magnetite Fe_3O_4) and $Fe^{2+}(Co,Zr)O$ (based on wustite $Fe_{1-\delta}O$ or $(Fe_xCo_{1-x})_{1-\delta}O$ complex oxide). The films with $x \geq 67$ at.% also exhibit the formation of α-FeCo(Zr,O) ferromagnetic nanoparticles or their ferromagnetically interacting agglomerations whose contribution increases with x. With an increase in the oxygen pressure ($P_O = (3.7÷5.0) \cdot 10^{-3}$ Pa) during the synthesis, only superparamagnetic particles of the $Fe^{3+}(Co,Zr)O$ complex oxide form over the whole range of experimental compositions [10, 17–19].

3.3. Thermal and field dependences of electrical resistivity of oxidized FeCoZr-PZT films

Typical thermal dependences of the electrical resistivity of oxidized FeCoZr-PZT films synthesized at $P_O = 3.2 \cdot 10^{-3}$ and $5.0 \cdot 10^{-3}$ Pa are shown in Figs. 3 and 4. For films synthesized at lower oxygen pressures the curves exhibit a negative thermal coefficient of electrical resistivity for compositions with $x < x_C$. This is also the case for the films with compositions beyond the percolation threshold at temperatures of below ≈ 100 K. This fact may indicate an activation mechanism of electrical conductivity in the test films.

However the experimentally observed curves cannot be approximated by a linear function in Mott's ($T^{-0.25}$) or Shelovskoi–Efros' ($T^{-0.5}$) coordinates and hence there is a more complex electrical conductivity mechanism in films with PZT matrix as compared with granular films of close compositions [11, 12, 20–24]. The thermal dependences of the electrical resistivity of the oxidized FeCoZr-PZT films with $x > x_C$ exhibit an abrupt transition to a positive thermal coefficient of electrical resistivity at above 100 K which testifies to the presence of a contribution from metallic conductivity. Furthermore as can be seen from Fig. 3 the change in the sign of the thermal coefficient of electrical resistivity occurs for the $(FeCoZr)_{69}(PZT)_{31}$

and $(FeCoZr)_{85}(PZT)_{15}$ films that exhibit an abrupt drop in the electrical conductivity in comparison with the $(FeCoZr)_{40}(PZT)_{60}$ and $(FeCoZr)_{54}(PZT)_{46}$ films. With an increase in the oxygen pressure during the synthesis the thermal curves exhibit positive thermal coefficients of electrical resistivity over the entire range of experimental compositions (Fig. 4). An increase in x is accompanied by a growth in the electrical conductivity, though less expressed as for less oxidized FeCoZr-PZT films discussed above (Fig. 3). The this specific behavior seems to originate from the complete oxidation of the nanoparticles as confirmed by EXAFS spectroscopy (Fig. 2) and Mossbauer spectroscopy data [10, 17, 18].

4. Conclusion

X-ray structural data showed that $(FeCoZr)_x(PZT)_{100-x}$ films synthesized at $P_O = 2.4 \cdot 10^{-3}$ Pa contain completely oxidized nanopartciles for the compositions $x < 50$ at.% and a combination of unoxidized α-FeCo(Zr,O) nanoparticles with completely oxidized nanoparticles for the compositions $x > 50$ at.%. Films deposited at $P_O = 3.7 \cdot 10^{-3}$ Pa contain only completely oxidized nanopartciles over the whole experimental composition range. Extended X-ray absorption fine structure spectros-
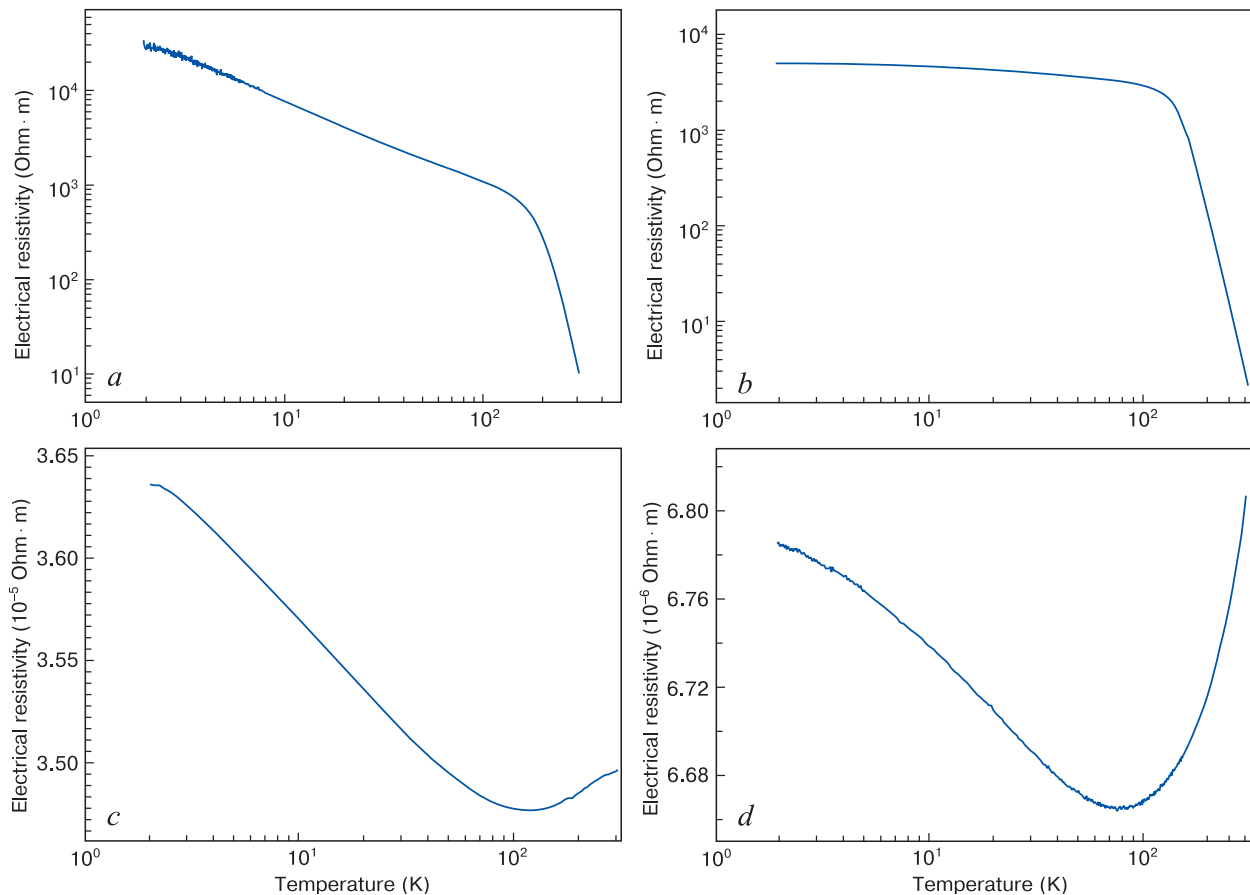

Figure 3. Thermal coefficients of electrical resistivity of oxidized films: (*a*) $(FeCoZr)_{40}(PZT)_{60}$, (*b*) $(FeCoZr)_{54}(PZT)_{46}$, (*c*) $(FeCoZr)_{69}(PZT)_{31}$ and (*d*) $(FeCoZr)_{85}(PZT)_{15}$ synthesized at $P_O = 3.2 \cdot 10^{-3}$ Pa

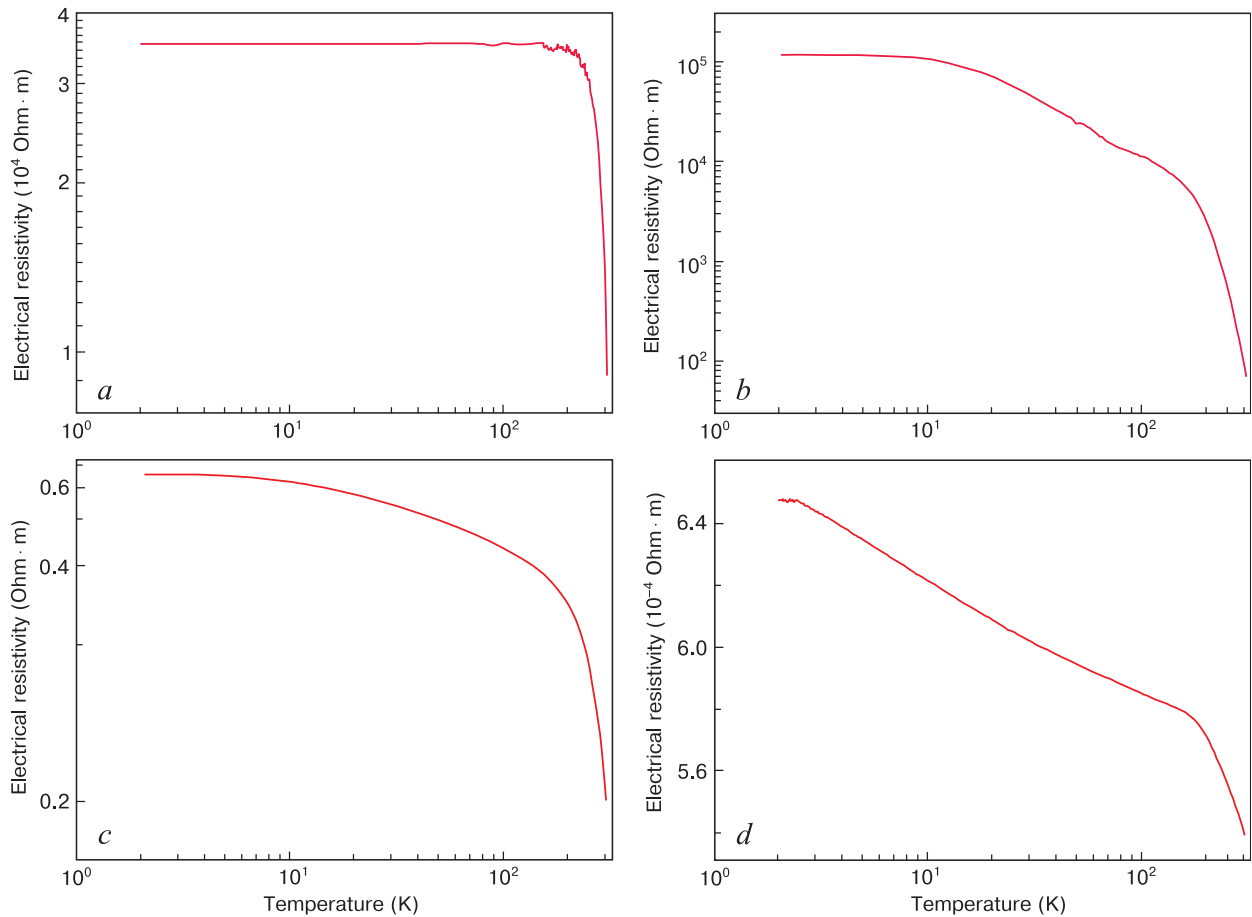**Figure 4.** Thermal coefficients of electrical resistivity of oxidized films: (*a*) (FeCoZr)$_{30}$ (PZT)$_{60}$, (*b*) (FeCoZr)$_{50}$(PZT)$_{50}$, (*c*) (FeCoZr)$_{64}$(PZT)$_{36}$ and (*d*) (FeCoZr)$_{81}$(PZT)$_{19}$ synthesized at $P_O = 5.0 \cdot 10^{-3}$ Pa

copy of iron and cobalt in (FeCoZr)$_x$(PZT)$_{100-x}$ films oxidized at $P_O = 2.4 \cdot 10^{-3}$ Pa showed that at $x \approx x_C$ the local neighborhood of iron and cobalt ions corresponds to that for almost completely oxidized FeCoZr nanoparticles whereas at $x > x_C$ it suggests the simultaneous presence of α-FeCo(Zr,O) cobalt-rich metallic alloy and iron oxides. The change in the position of the iron and cobalt EXAFS peaks after Fourier transformation for the FeCoZr-PZT films oxidized at $P_O = 3.2 \cdot 10^{-3}$ Pa suggests a transition of the local neighborhood of the iron ions from an oxide-typical one to a metallic one with an increase in x. The local neighborhood of cobalt is in this case typically metallic for all the experimental compositions. For the highest oxygen pressure ($P_O = 5.0 \cdot 10^{-3}$ Pa) during film synthesis the local neighborhood of the iron and cobalt ions consists of oxygen ions and this suggests the complete oxidation of the nanoparticles.

The thermal dependences of electrical resistivity of the oxidized (FeCoZr)$_x$(PZT)$_{100-x}$ films with 40 at.% $\leq x < 85$ at.% synthesized at $P_O = 3.2 \cdot 10^{-3}$ Pa suggest a negative thermal coefficient of electrical resistivity at 2–300 K for $x \leq 54$ at.% and a change in the sign of the thermal coefficient of electrical resistivity to positive at 100–300 K for $x \geq 69$ at.%. The observed transition from a negative to a positive

thermal coefficient of electrical resistivity can be accounted for by a change in the phase composition, e.g. by the oxidation degree of the FeCoZr nanoparticles. For example at compositions below the percolation threshold (at $x \geq 69$ at.%) the films usually contain Fe^{2+}Fe^{3+}(Co,Zr)O complex oxidesnanoparticles whereas at higher x they exhibit the formation of Fe^{2+}Fe^{3+}(Co,Zr) O complex oxides and α-FeCo(Zr,O) ferromagnetic nanoparticles that provide for the metallic conductivity mechanism.

For the (FeCoZr)$_x$(PZT)$_{100-x}$ films synthesized at higher oxygen pressures $P_O = 5.0 \cdot 10^{-3}$ Pa the sign of the thermal coefficient of electrical resistivity is negative over the whole experimental concentration range due to the complete oxidation of the nanopartciles and the formation of the Fe^{2+}Fe^{3+}(Co,Zr)O complex oxides.

Acknowledgments

References

1. Zolotukhin I.V., Stognei O.V. *Fizika nanosistem: grafeny i granu-lirovannye nanokompozity* [Physics of nanosystems: graphenes and granular nanocomposites]. Voronezh: Voronezh State Technical University, 2011, 226 p. (In Russ.)

2. Sitnikov A.V. *Electrical and magnetic properties of nanoheteroge-neous metal-dielectric systems:* Dis. Dr. Sci. (Phys.-Math.). Voronezh, 2009, 280 p. (In Russ.)

3. Blinov M.I., Shakhov M.A., Rylkov V.V., Lähderant E., Prudnikov V.N., Nikolaev S.N., Sitnikov A.V., Granovsky A.B. Magnetoresistance of $(Co_{40}Fe_{40}B_{20})_x(SiO_2)_{100-x}$ and $(Co_{84}Nb_{14}Ta_2)_x(Al_2O_3)_{100-x}$ nanocomposites below the percolation threshold in pulsed magnetic fields. *J. Magn. Magn. Mater.*, 2019; 469: 155–160. https://doi.org/10.1016/j.jmmm.2018.08.023

4. Kalinin Yu.E., Makagonov V.A., Sitnikov A.V., Granovsky A.B. Electrical properties of ferromagnetic-insulator nanocomposites. *Eur. Phys. J. Web Conf.*, 2018; 185: 03001. https://doi.org/10.1051/epjconf/201818503001

5. Antonets I.V., Kotov L.N., Golubev E.A., Kalinin Yu.E., Sitnikov A.V. The structure, conductive properties, and reflective prop-erties of amorphous granular $(Co_{45}Fe_{45}Zr_{10})_x(ZrO)_{1-x}$ composite films. *Tech. Phys.*, 2017; 62: 261–269. https://doi.org/10.1134/S1063784217020025

6. Kulyk M.M., Kalita V.M., Lozenko A.F., Ryabchenko S.M., Stognei O.V., Sitnikov A.V., Korenivski V. Magnetic properties and aniso-tropic coercivity in nanogranular films of Co/Al_2O_3 above the perco-lation limit. *J. Phys. D: Appl. Phys.*, 2014; 47(34): 345002. https://doi.org/10.1088/0022-3727/47/34/345002

7. Antonets I.V., Kotov L.N., Golubev E.A., Kalinin Yu.E., Sit-nikov A.V. Nanostructure and electrical conductivity of amorphous granular $(Co_{45}Fe_{45}Zr_{10})_x(Al_2O_3)_{1-x}$ composite films. *Tech. Phys.*, 2016; 61(3): 416–423. https://doi.org/10.1134/S1063784216030038

8. Mikhailovskii Yu.O., Prudnikov V.N., Ryl'kov V.V., Cher-noglazov K.Yu., Sitnikov A.V., Kalinin Yu.E., Granovskii A.B. Logarithmic temperature dependence of electrical resistivity of $(Co_{41}Fe_{39}B_{20})_x(AlO)_{100-x}$ nanocomposites. *Phys. Solid State*, 2016; 58(3): 444–446. https://doi.org/10.1134/S1063783416030227

9. Kasiuk J.V., Fedotova J.A., Marszalek M., Karczmarska A., Mitu-ra-Nowak M., Kalinin Yu.E., Sitnikov A.V. Effect of oxygen pressure on phase composition and magnetic structure of $FeCoZr-Pb(ZrTi)O_3$ nanocomposites. *Phys. Solid State*, 2012; 54: 178–184. https://doi.org/10.1134/S1063783412010179

10. Kołtunowicz T.N., Fedotova J.A., Zhukowski P., Saad A., Fedo-tov A., Kasiuk J.V., Larkin A.V. Negative capacitance in (FeCoZr)–(PZT) nanocomposite films. *J. Phys. D: Appl. Phys.*, 2013; 46(12): 125304. https://doi.org/10.1088/0022-3727/46/12/125304

11. Saad A., Fedotova J., Nechaj J., Szilagyi E., Marszalek M. Tun-ing of magnetic properties and structure of granular $FeCoZr-Al_2O_3$ nanocomposites by oxygen incorporation. *J. Alloys Compd.*, 2009; 471(1–2): 357–363. https://doi.org/10.1016/j.jallcom.2008.03.120

12. Fedotova J.A., Przewoznik J., Kapusta Cz., Milosavljević M., Kasiuk J.V., Zukrowski J., Sikora M., Maximenko A.A., Szepi-etowska D., Homewood K.P. Magnetoresistance in $FeCoZr-Al_2O_3$ nanocomposite films containing "metal core-oxide shell" nanogran-ules. *J. Phys. D: Appl. Phys.*, 2011; 44(49): 495001. https://doi.org/10.1088/0022-3727/44/49/495001

13. Gridnev S.A., Kalgin A.V. Phase transitions in $xPbZr_{0.53}Ti_{0.47}O_{3-(1-x)}$ $Mn_{0.4}Zn_{0.6}Fe_2O_4$ magnetoelectric composites. *Phys. Solid State*, 2009; 51: 1458–1461. https://doi.org/10.1134/S1063783409070324

14. Naĭden E.P., Zhuravlev V.A., Itin V.I., Terekhova O.G., Maga-eva A.A., Ivanov Yu.F. Magnetic properties and structural parame-ters of nanosized oxide ferrimagnet powders produced by mechano-chemical synthesis from salt solutions. *Phys. Solid State*, 2008; 50: 894–900. https://doi.org/10.1134/S1063783408050156

15. Shi Y., Ding J., Yin H. $CoFe_2O_4$ nanoparticles prepared by the mechanochemical method. *J. Alloys Compd.*, 2000; 308(1–2): 290–295. https://doi.org/10.1016/S0925-8388(00)00921-X

16. Fedotova J., Kasiuk J., Przewoznik J., Kapusta Cz., Svito I., Ka-linin Yu., Sitnikov A. Effect of oxide shells on the magnetic and magnetotransport characteristics of oxidized FeCoZr nanogranules in Al_2O_3. *J. Alloys Compd.*, 2011; 509(41): 9869–9875. https://doi.org/10.1016/j.jallcom.2011.07.066

17. Kasiuk J., Fedotova J., Przewoźnik J., Kapusta Cz., Sikora M., Żukrowski J., Grce A., Milosavljević M. Oxidation controlled phase composition of FeCo(Zr) nanoparticles in CaF_2 matrix. *Ma-ter. Character.*, 2016; 113: 71–81. https://doi.org/10.1016/j.mat-char.2016.01.010

18. Koltunowicz T.N., Zukowski P., Boiko O., Saad A., Fedotova J.A., Fedotov A.K., Larkin A.V., Kasiuk J. AC hopping conductance in nanocomposite films with ferromagnetic alloy nanoparticles in a $Pb-ZrTiO_3$ matrix. *J. Electron. Mater.*, 2015; 44(7): 2260–2268. https://doi.org/10.1007/s11664-015-3685-9

19. Kumar H., Olivi L., Aquilanti G., Ghosh S., Srivastava P., Ka-biraj D., Avasthi D. K. Stabilization of FeCo alloy phase in Fe-Co-SiO_2 nanocomposites. *Adv. Mater. Lett.*, 2013; 4(6): 390–397. https://doi.org/10.5185/amlett.2012.ib.101

20. Zukowski P., Koltunowicz T.N., Boiko O., Bondariev V., Czarnac-ka K., Fedotova J.A., Fedotov A.K., Svito I.A. Impedance model of metal-dielectric nanocomposites produced by ion-beam sputtering in vacuum conditions and its experimental verification for thin films of $(FeCoZr)_x(PZT)_{(100-x)}$. *Vacuum*, 2015; 120(B): 37–43. https://doi.org/10.1016/j.vacuum.2015.04.035

21. Zukowski P., Koltunowicz T.N., Bomdariev V., Fedotov A.K., Fedotova J.A. Determining the percolation threshold for $(FeCoZr)_x(CaF_2)_{(100-x)}$ nanocomposites produced by pure argon ion-beam sputtering. *J. Alloys Compd.*, 2016; 683: 62–66. https://doi.org/10.1016/j.jallcom.2016.05.070

22. Fujiwara Y., Matsuda H., Sato K., Jimbo M., Kobayashi T. Magne-toresistance and electronic structure of granular films with MgO or MgF_2 matrices. *J. Phys.: Conf. Ser.*, 2011; 266(1): 012087. https://doi.org/10.1088/1742-6596/266/1/012087

23. Peng D.L., Wang J.B., Wang L.S., Liu X.L., Wang Zh.W., Chen Y.Zh. Electron transport properties of magnetic granular fil-ms. *Sci. China Phys. Mech. Astron.*, 2013; 56: 15–28. https://doi.org/10.1007/s11433-012-4969-1

24. Gerke M.N., Istratov A.V., Bukharov D.N., Novikova O.A., Skryabin I.O., Arakelian S.M. Studying the structure and elec-trical conductivity of thin granular bimetallic films. *Bull. Russ. Acad. Sci.: Physics*, 2017; 81: 1387–1390. https://doi.org/10.3103/S1062873817120127